

Three-Dimensionally Homoconjugated Carbon-Bridged Oligophenylenevinylene for Perovskite Solar Cells

Qifan Yan, Yunlong Guo, Anna Ichimura, Hayato Tsuji, and Eiichi Nakamura

J. Am. Chem. Soc., **Just Accepted Manuscript** • DOI: 10.1021/jacs.6b04002 • Publication Date (Web): 05 Aug 2016

Downloaded from <http://pubs.acs.org> on August 6, 2016

Just Accepted

“Just Accepted” manuscripts have been peer-reviewed and accepted for publication. They are posted online prior to technical editing, formatting for publication and author proofing. The American Chemical Society provides “Just Accepted” as a free service to the research community to expedite the dissemination of scientific material as soon as possible after acceptance. “Just Accepted” manuscripts appear in full in PDF format accompanied by an HTML abstract. “Just Accepted” manuscripts have been fully peer reviewed, but should not be considered the official version of record. They are accessible to all readers and citable by the Digital Object Identifier (DOI®). “Just Accepted” is an optional service offered to authors. Therefore, the “Just Accepted” Web site may not include all articles that will be published in the journal. After a manuscript is technically edited and formatted, it will be removed from the “Just Accepted” Web site and published as an ASAP article. Note that technical editing may introduce minor changes to the manuscript text and/or graphics which could affect content, and all legal disclaimers and ethical guidelines that apply to the journal pertain. ACS cannot be held responsible for errors or consequences arising from the use of information contained in these “Just Accepted” manuscripts.

Three-Dimensionally Homoconjugated Carbon-Bridged Oligophenylenevinylene for Perovskite Solar Cells

Qifan Yan,[†] Yunlong Guo,* Anna Ichimura, Hayato Tsuji,*[†] Eiichi Nakamura*

Department of Chemistry, The University of Tokyo, 7-3-1 Hongo, Bunkyo-ku, Tokyo 113-0033, Japan.

ABSTRACT: Stabilization of the radical cationic state of a donor molecule by 3-D homoconjugation was probed using a substituted carbon-bridged oligophenylenevinylene backbone (COPV or 5,5-diaryl-indeno[2,1-*a*]indenes). For molecules bearing electron-donating groups as the 5,5-aryl moieties, a one-electron oxidation of the COPV backbone results in delocalization of the cationic charge over the whole molecule with a small reorganization energy. The compounds forming a stable radical cation by 3-D homoconjugation produce a uniform amorphous film and show high short-circuit current, high fill factor, and hence high power-conversion efficiency when used as a hole-transporting layer of an organic-inorganic hybrid lead perovskite solar cell. This material thus shows a performance and stability in air comparable to that obtained by the benchmark material, **spiro-MeOTAD**.

INTRODUCTION

Stabilization of negative charge on a 3-D π -scaffold has attracted considerable attention from chemists since the discovery of the utility of fullerenes as electron-accepting material in organic and perovskite solar cells (SCs). Such 3-D molecules used as carrier-transporting materials tend to have a small reorganization energy and to give amorphous morphology suitable for carrier transport in a film. On the other hand, there has been a paucity of studies on the potential of 3-D stabilization of positive charge for hole transportation where, chemically speaking, a radical cation of hole-transporting material plays the role. Having found¹ that a carbon-bridged oligophenylenevinylene backbone (COPV-1 or 5,5-diaryl-indeno[2,1-*a*]indenes, denoted as COPV hereafter) provides a structurally robust 2-D π -scaffold (cyan, Figure 1a), we were intrigued by the possibility of 3-D homoconjugative stabilization of a radical cation through installation of additional electron-donating aminophenyl groups orthogonal to the plane of the COPV π -system (Figure 1a). We report here the synthesis, properties and SC application of the new electron-rich π -system (**1–3**; Figure 1b) examined for the effects of the 3-D homoconjugative stabilization of a radical cationic state. The compounds form an effective, amorphous hole-transporting layer (HTL) for a thin-film semitransparent² lead perovskite SC device³, which are already finding use in "solar window" applications.⁴ The perovskite SCs using **1–3** show a level of power-conversion efficiency (PCE) and stability in air comparable to that using popularly employed **spiro-MeOTAD** (Figure 1b, bottom)—a benchmark of hole-transporting material.⁵ Reference compounds **4–6**, which have only the flat 2-D conjugated system, were found to perform poorly as an HTL in spite of the similarity of their oxidation potentials to those of **1–3**. Compounds **1–3** form a stable radical cation and produce a uniform amorphous film, and hence showed high short-circuit current (J_{sc}), high fill factor (FF) and hence high PCE. Compound **4**, which forms an amorphous film but is incapable of homoconjugative stabilization of a radical cation, showed

high J_{sc} but poor FF. Compounds **5** and **6**, which form a crystalline film and are incapable of radical cation stabilization, showed poor performance for J_{sc} , open-circuit voltage (V_{oc}), FF and PCE. A simple fluorene **7** lacking the ability of stabilizing its oxidized form showed a low performance and poor stability in air.

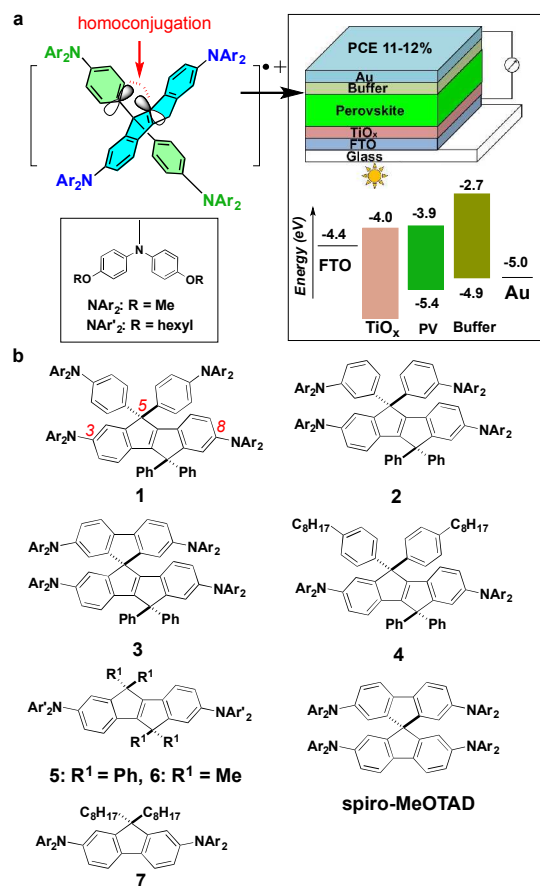


Figure 1. SC device configuration and molecular structures in our study. a) Schematic illustration of three-dimensional

once the COPV moiety is oxidized (PV^{1+}). Likewise, oxidation of the 4-aminoaryl groups in **1** and **2** becomes so difficult that they are oxidized only after the second oxidation of the COPV core (PV^{2+}).

Table 1. Photophysical and electrochemical data^a

compd	$\lambda_{\text{abs}}/\text{nm}$	$\epsilon/10^4 \text{ M}^{-1} \text{ cm}^{-1}$	$\lambda_{\text{fl}}/\text{nm}$	Φ_{fl}	τ/ns	E_{ox}/V
1	417/435	4.3/4.3	465	0.87	2.03	-0.05, 0.18, 0.30 (2e)
2	418/435	4.7/4.6	467	0.91	2.06	-0.04, 0.21, 0.32 (2e)
3	397/431	6.4/4.2	463	0.87	2.02	-0.03, 0.14, 0.22, 0.33
4	417/433	4.4/4.4	466	0.83	1.86	-0.04, 0.17
5	420/435	4.7/4.7	470	0.80	1.93	-0.05, 0.17
6	402/416	4.1/4.0	447	0.84	1.53	-0.15, 0.07
7	388	3.5	417	0.50	1.27	-0.03, 0.26

^a Φ_{fl} (fluorescence quantum yield) was determined using an absolute method; τ (fluorescence lifetime) was measured using a time-correlated single-photon counting method with a 405 nm NanoLED for **1–6** and a 365 nm NanoLED for **7**, as excitation source and fitted single exponentially with χ^2 from 0.89–1.21; E_{ox} was calculated against Fc^+/Fc couple as external reference.

3. Characteristics of neutral and radical cation

Absorption titration experiments on chemical oxidation provided further support for the homoconjugation between the radical cation of the COPV moiety and the 4-aminophenyl group in **3**. Thus, a solution of compounds **3**, **4** and **7** in chlorobenzene was treated with aliquots of nitrosonium hexafluorophosphate (NO^+PF_6^-), monitored with UV–vis absorption (Figure 3 and Figure S1). Upon addition of the oxidant to a solution of the aminofluorene **7**, a new peak at 522 nm rose at the expense of the band at 397 nm of the neutral molecule (Figure 3a). The 522-nm peak is due to the SOMO-to-LUMO transition of the fluorene radical cation. Similarly to the previously reported parent COPV-1,^{1a} the radical cation of **4** shows absorptions at 665 nm and 616 nm due to 0–0 and 0–1 transitions, respectively (Figure 3b). In **3** (Figure 3c), where fluorene and indeno[2,1-*a*]indene moieties are homoconjugated, the three bands developed simultaneously, indicating that both the COPV and the geminal 4-aminophenyl groups contribute to this spectral change because of formation of the radical cation (see SI for full range UV–vis–NIR spectra of **1–5** upon oxidation).

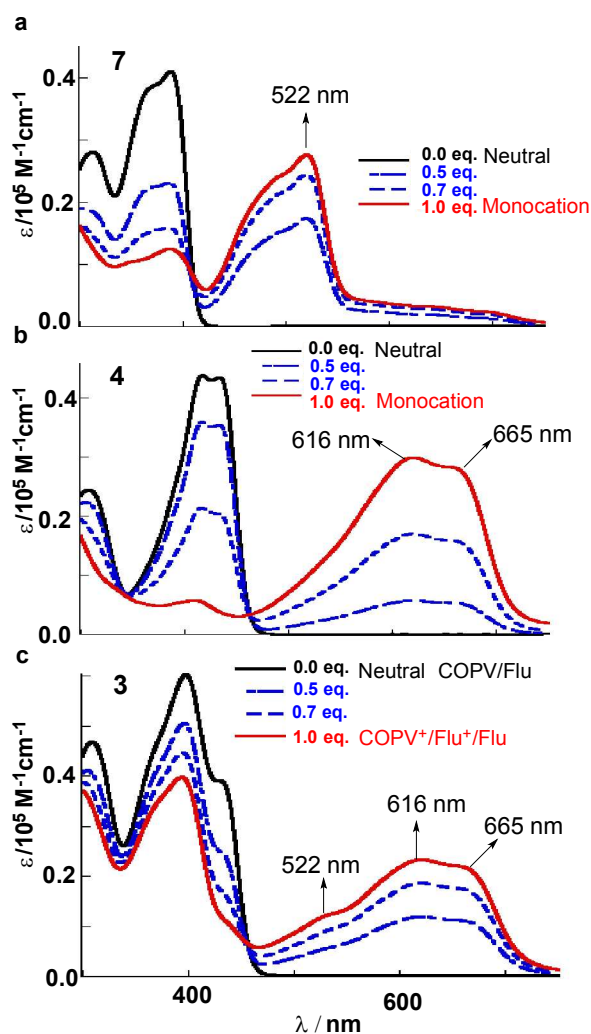


Figure 3. Titration experiments monitored by UV–vis absorption spectra of a solution in PhCl at 5 μM upon adding NO^+PF_6^- : (a) **7**, (b) **4** and (c) **3**. Arrows indicate local maxima.

Density functional theory (DFT) calculations on both neutral and radical cation states of COPV **1–6** were carried out at the B3LYP/6-31G(d,p) theory level (details in Supporting Information, Figure S2–S7). The calculated total positive charge on the two aminophenyl groups in the radical cations of **1**, **2** and **3** are 0.27, 0.20 and 0.34, respectively, whereas that of **4** was only 0.08. Similarly, the spin density of the radical cation of **3** delocalizes significantly on the fluorene part, as shown in Figure S8. This is in stark contrast to compound **4**; the spin density of 4^+ resided mainly on the COPV moiety (see SI for HOMOs of the neutral compounds).

Careful comparison of the charge distribution between neutral and radical cation and the geometry parameters supports the existence of homoconjugation in the radical cation (Table 2). For example, the reorganization energies upon formation of the radical cations for **3** were clearly smaller than those for **4–6** (Table 2, second column). Upon removal of one electron from COPV **1–5**, the distance l shown by a red arrow in Figure 4a shortens most significantly for **1** and **3**. In agreement with this structural change, the radical cations of **1** and **3** showed a larger positive charge on the geminal aryl groups. The compounds **4** and **5** lack electron-donating diamine groups on the phenyl groups, and hence the phenyl groups cannot take part in homoconjugation when the compounds are oxidized (see Figure 2b, DPV). Smaller

homoconjugation in **4–6** is seen in the smaller values of the positive charge and the distance reduction in Table 2.

Table 2. DFT analysis of radical cations of **1–6** at the B3LYP/6-31G(d,p) level of theory.^a

Compound	Charge on C5 substituents	Reorganization energy/eV	Distance reduction/Å (%)
1	0.27	0.28	0.015 (0.60%)
2	0.20	0.27	0.003 (0.13%)
3	0.34	0.21	0.009 (0.36%)
4	0.08	0.25	0.004 (0.17%)
5	0.07	0.25	0.004 (0.14%)
6	0.06	0.29	0.001 (0.04%)

^a The charge on the C5 substituents refers to the difference between the neutral and radical cationic states. Distance reduction refers to the shortening of the distance between the *ipso*-phenyl carbon atom bonded to C5 and the vinyl carbon bonded to C5, as indicated by a red arrow in Figure 4a.

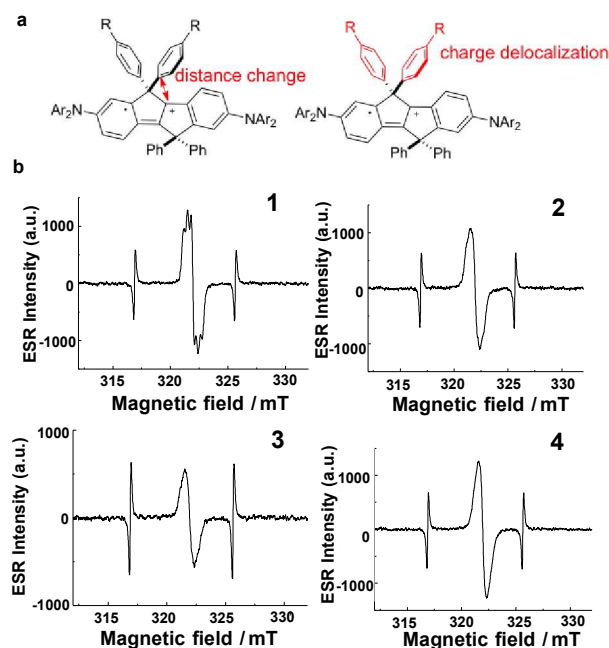


Figure 4. The properties of radical cations. (a) Illustration of the carbon–carbon distance and charge delocalization in the radical cation. (b) ESR spectra of the radical cations of **1–4** in PhCl.

The ESR spectra of **1–4** in solution verified the radical nature of the oxidized species (Figure 4b). The radical cation of reference **4** showed an ESR signal with a *g* value of 2.00040, which is typical for organic radicals. Radical cations of **1–3** also exhibited similar *g* values of 2.00039, 2.00038 and 2.00046, respectively. It is notable that the ESR spectrum of the radical cation of **1** displayed pronounced hyperfine structure caused by intervalence charge transfer with diaryl amino groups on C5 implying effective interactions between COPV moiety and substituents in **1⁺**. Broadened ESR signal were observed for **2⁺** and **3⁺**, suggesting delocalized radical. In comparison, ESR spectrum of **4⁺** displayed a much sharper peak without hyperfine structure, indicative of a less delocalized radical (Figure 4b).^{10b} These results further suggest that the homoconjugation is much more pronounced in the radical cations of **1–3** than that of **4**.

4. SCs based on COPV as HTL

Above studies indicate COPV's potential usefulness as HTL materials, if the orbital energy levels match with the potentials of PV and Au electrode. It was indeed the case. By photoemission yield spectroscopy, we determined the HOMO level of all of the compounds in their film state to be -4.9 eV (-4.8 eV for **6**). From the onset of the UV–vis absorption spectra, we determined the band gap (Table S7 and Figure 2a). These data suggest that they are suitable for blocking electrons and transporting holes.

Measurements of hole mobility and conductivity for doped and undoped compounds **1–7** as well as **spiro-MeOTAD** indicated that doping of our compounds slightly increases the mobility and the conductivity, and the doped data are comparable to those of **spiro-MeOTAD** (in the order of 10^{-5} $\text{cm}^2 \text{V}^{-1} \text{s}^{-1}$ and 10^{-6} S/cm, respectively). These data obtained for ITO/PEDOT:PSS/HTL(or HTL-doped)/Au are shown in Figure S9-S10 and Table S8.

Encouraged by the theoretical and experimental data suggesting good hole-transporting ability of a film of COPV **1–3**, we examined their potential as a buffer layer in thin-film perovskite SC devices, using **4–7** as references. For this purpose we employed a planar TiO_x as an ETL in our test semitransparent SC devices, which we could reproducibly fabricate in our hand. A solution of the COPVs and dopants, Li-TFSI (lithium bis(trifluoromethane sulfonyl) imide) and TBP (2,6-di-*tert*-butylpyridine), were spin-coated on a lead perovskite layer prepared as reported previously.¹¹ The whole SC device consists of FTO/ TiO_x (45 nm)/ $\text{CH}_3\text{NH}_3\text{PbI}_{3-x}\text{Cl}_x$ (230 nm)/buffer layer (200 nm)/Au (80 nm)/CYTOP and tested under AM 1.5G illumination with a power density of 100 mW cm^{-2} . This device shows an average transparency of ca. 25% without metal electrode.

As shown in Figure 5a, the device consists of very uniform layers of perovskite and doped compound **1** (**1**-doped) as imaged with a low landing voltage scanning electron microscopy (SEM). Such an SEM allows us to image directly the surface of conducting and insulating materials without metal coating that is usually required for conventional SEM imaging (to avoid sample charging).

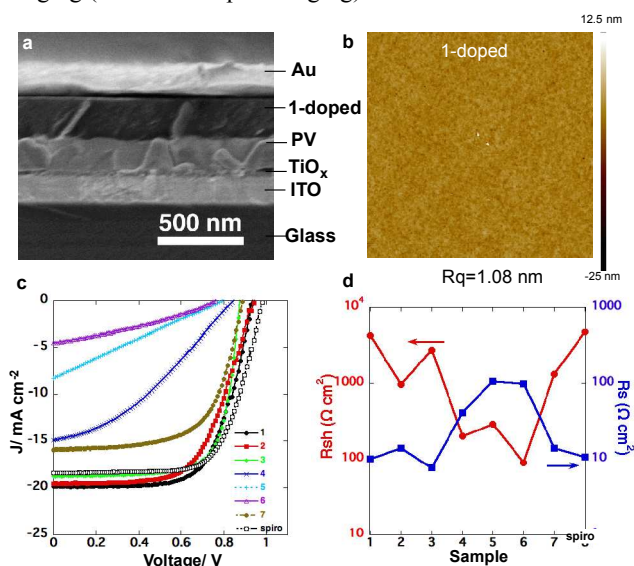


Figure 5. Cross-section image of SC, surface morphology of doped compound **1** (**1**-doped) and J - V characteristics of SC devices under AM 1.5G illumination. (a) Cross-section SEM image of device. Perovskite, TiO_x and ITO layers containing heavy metals are seen as gray layers because they emit more

backscattered electrons than organic materials, and hence the organic HTL is seen to be darker. (b) AFM image of compound **1** (I-doped) (c) J - V curves and (d) relationships between different SCs and shunt resistance, R_{sh} , as well as series resistance, R_s .

Table 3. Performance parameters of thin-film perovskite SCs using different buffer layers (see text for details).

Compound	$J_{sc}/$ mA cm^{-2}	$V_{oc}/$ V	FF	PCE/ %	$R_{sh}/$ $\text{k}\Omega \text{ cm}^2$	$R_s/\Omega \text{ cm}^2$
1	19.9	0.93	0.66	12.3	4.26	10.1
2	19.6	0.94	0.61	11.2	0.97	13.8
3	18.7	0.88	0.73	12.0	2.70	7.7
4	14.9	0.85	0.35	4.4	0.20	40.5
5^a	4.5	0.76	0.33	1.1	0.29	106
6	8.3	0.80	0.24	1.6	0.09	98
7	15.9	0.89	0.63	8.9	1.30	14.0
Spiro-MeOTAD	18.4	0.98	0.68	12.2	4.76	10.6

^a Doped with FK209. R_{sh} and R_s obtained from the J - V curve in Figure 5.

As shown in the bottom of Table 3, the reference perovskite SC system, studied here for a popular buffer, **spiro-MeOTAD**, shows a PCE of 12.2% with J_{sc} of 18.4 mA cm^{-2} , V_{oc} of 0.98 V and FF of 0.68, as shown in the bottom of Table 3, and the efficacies of the homoconjugated compounds **1–3** were found to be comparable. For example, a **1**-based device showed a PCE of 12.3% with J_{sc} of 19.9 mA cm^{-2} , V_{oc} of 0.93 V and FF of 0.66. The highest performance of **1** coincides well with the highest degree of homoconjugation in the radical cationic state as discussed above.

COPV **1–4** behave similarly in terms of the amorphous nature of the films, as shown by the lack of XRD peaks and by absorption spectra almost identical to those in solution (Figure S11 and S12). Therefore, we expect a smooth interface with perovskite and hence a high ability of the film to collect charge at the interface with the perovskite film. In Figure 5b and Figure S13 is shown the very smooth surface of HTL of doped compound **1** (root mean square roughness (Rq) of 1.08 nm) as studied by atomic-force microscopy (AFM). This is supported by the high J_{sc} values of 14.9–19.9 mA cm^{-2} for **1** to **4** (Table 3). However, reference **4** differs markedly from **1–3** for its very small FF value of 0.35, large R_s of 40.5 $\Omega \text{ cm}^2$ and PCE of 4.4%, indicative of poor hole-conducting ability. A device using the fluorene reference compound **7** showed PCE of 8.9% (best data among multiple runs), which is 26% lower than a spiro-MeOTAD device. Meanwhile, the stability of SC using compound **7** was much worse than other HTLs: The PCE value decreased to 20% of original value after 48 h in air (Figure 6a) accompanying the color the PV film (Figure 6b). Note that the stability of the devices using the compound **1** and **Spiro-MeOTAD** was found to be comparable. We can ascribe these to the lack of homoconjugative stabilization of the radical cation, which plays a key role in the increase of the device stability and the hole transporting ability of HTL.

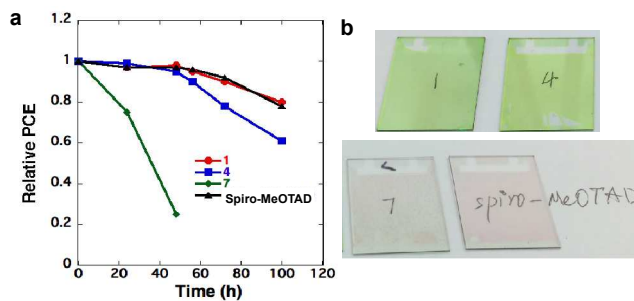


Figure 6. Stability of the solar cells using various HTL materials. (a) Relative PCE of solar cells based on different HTLs and (b) the appearance of various devices after 48 h in air with humidity about 40 %.

In contrast to **1–4**, **5** and **6** form a crystalline film, as shown by the appearance of XRD diffraction peaks (**5**, $2\theta = 3.47^\circ$, $d = 2.54 \text{ nm}$; **6**, $2\theta = 6.33^\circ$, $d = 1.39 \text{ nm}$; see Figure S11), which would cause poor contact with the perovskite layer and insufficient charge collection. Therefore, we found a small R_{sh} , large R_s and very small J_{sc} of 4.5 and 8.3 mA cm^{-2} for **5** and **6**, respectively (Table 3).

CONCLUSION

In summary, we have probed the origin of the high hole-transporting ability of popular **spiro-MeOTAD** and found that stabilization of a radical cationic state through 3-D homoconjugation can serve as a generally useful strategy for the design of an amorphous and efficient HTL in a perovskite SC. A few key features of the 3-D COPV system have been identified to be critical for good performance. First, the 3-D homoconjugated system has intrinsically smaller reorganization energy than the flat 2-D system and hence reorganizes to higher charge transporting ability. Second, the multiply substituted system allows tuning of the energy levels of HOMO and LUMO of the film through structural changes of the donor groups to obtain maximum hole conductivity. We envisage that longer COPV systems will provide further electronic tuning.⁷ Third, a 3-D system tends to form an amorphous film and hence produces a smoother interface with neighboring layers to increase the current density. The high performance of **1**, comparable with that of **spiro-MeOTAD**, supports the importance of 3-D homoconjugation.¹² Overall, the homoconjugation strategy based on the COPV skeleton improves charge carrier transportation without affecting the energy levels of the HOMO and LUMO of the HTL and hence is useful for the control of carrier injection. As combined with recent information on the PV formation mechanism,¹³ we can now have a prospect of designing PV devices through rational chemical design of the active layer and interlayers.

EXPERIMENTAL SECTION

General information for synthetic procedures. All oxygen- and moisture-sensitive reactions were performed under a nitrogen atmosphere using the standard Schlenk method, lithium/naphthalene reagent was prepared under an argon atmosphere. Analytical thin-layer chromatography (TLC) was performed using glass plates precoated with 0.25 mm, 230–400 mesh silica gel impregnated with a fluorescent indicator (254 nm). TLC plates were visualized by exposure to ultraviolet light (UV). Flash column chromatography was performed on Kanto silica gel 60 (spherical, neutral, 140–325

mesh).¹⁴ Chemicals were purchased from Tokyo Kasei Co. and Aldrich Inc., and used as received unless otherwise indicated. Reagent grade tetrahydrofuran (THF) and toluene (Tol) were purified using a solvent-purification system. The following compounds were prepared following the literature: bis(4-octylphenyl)methanone,¹⁵ bis(4-bromophenyl)methanone,¹⁶ bis(3-bromophenyl)methanone¹⁷ and CuBr₂/Al₂O₃.¹⁸ ¹H and ¹³C NMR spectra were recorded on a Bruker US-500 (500 MHz) NMR spectrometer, using CDCl₃ or C₆D₆ as the solvent unless otherwise noted. Chemical shifts in ¹H and ¹³C NMR spectra were reported in parts per million (ppm, δ scale). Chemical shifts of ¹H signals were referenced with TMS (0 ppm) or residual C₆D₅H (7.16 ppm) as standards, and those of ¹³C signals were referenced with CDCl₃ (77.16 ppm) or C₆D₆ (128.06 ppm).¹⁹ The data are presented as follows: chemical shift, multiplicity (s = singlet, d = doublet, t = triplet, q = quartet, m = multiplet and/or multiple resonances, br = broad), coupling constant in hertz (Hz) and integration. Melting points of solid materials were determined on a Mel-Temp II capillary melting-point apparatus and are uncorrected. Mass spectra were obtained on a Bruker micrOTOF mass spectrometer. SEM imaging was conducted on an FEI Magellan 400L at a landing voltage of 1 kV under a reduced pressure of 5×10^{-5} Pa. AFM observations of PV thin-films were carried out on Bruker Multimode 8 instrument in air.

General procedure for lithium-induced reductive cyclization and intramolecular Friedel–Crafts cyclization reaction. A Schlenk tube charged with lithium (2.5 equiv to compound **8**) and naphthalene (2.5 equiv to compound **8**) was evacuated and back-filled with argon three times, then dry THF (0.25 mL per mg of lithium) was added. The tube was sealed under an argon atmosphere and the reaction mixture was stirred at room temperature for 5 h until the lithium was depleted. A Schlenk tube charged with compound **8** was evacuated and back-filled with nitrogen three times, then dry THF (the same for lithium) was added. The solution of **8** was added to lithium/naphthalene dropwise, and stirred at room temperature for 30 min before the corresponding ketone was added under nitrogen flow. The reaction mixture was stirred at room temperature for another 30 min before being quenched with a few drops of NH₄Cl (aq. saturated). The crude product was placed on a short column of silica gel with dichloromethane (DCM). After removal of solvents under vacuum, the crude tertiary alcohol was dissolved in carbon tetrachloride (0.4 mL per mg of **8**) without further purification, and boron trifluoride ether complex (2 μ L per mg of **8**) was added. The reaction mixture was stirred at room temperature for 30 min (compounds **9–12**) or at 70 °C for 3 h (compound **13**) before being quenched with methanol. After removal of solvents under vacuum, column chromatography over silica gel eluted with hexane/DCM afforded the desired **9–13** as white solids.

Compound **9** was prepared following the reported procedure.¹⁵

Compound **10** (70% from **8**). Mp: >250 °C. ¹H NMR (500 MHz, CDCl₃) δ 7.43–7.45 (m, 1H), 7.33–7.38 (m, 5H), 7.10–7.26 (m, 20H). ¹³C NMR (125 MHz, CDCl₃) δ 157.4, 156.0, 142.6, 141.5, 138.4, 137.9, 128.6, 128.5, 127.7, 127.4, 126.4, 126.3, 125.4, 121.4, 120.6, 63.4, 62.3. HRMS (APCI–TOF): Calcd for C₄₀H₂₆Br₂, 664.0401 (M⁺), found, 664.0422.

Compound **11** (62% from **8**). Mp: >250 °C. ¹H NMR (500 MHz, CDCl₃) δ 7.43–7.45 (m, 1H), 7.35–7.41 (m, 5H), 7.11–

7.30 (m, 20H). ¹³C NMR (125 MHz, CDCl₃) δ 157.5, 156.3, 156.0, 154.2, 144.6, 142.5, 138.4, 137.8, 131.3, 130.6, 130.3, 128.7, 128.5, 127.8, 127.5, 127.2, 127.1, 126.4, 125.4, 122.9, 121.4, 120.7, 63.4, 62.6. HRMS (APCI–TOF): Calcd for C₄₀H₂₆Br₂, 664.0401 (M⁺), found, 664.0414.

Compound **12** was precipitated from carbon tetrachloride and washed with methanol to give the product with satisfactory purity as a white solid (78% from **8**). ¹H NMR (500 MHz, CDCl₃) δ 7.42–7.43 (m, 2H), 7.29–7.31 (m, 8H), 7.22–7.25 (m, 12H), 7.17–7.19 (m, 2H), 7.09–7.15 (m, 4H).

Compound **13** (73% from **8**). Mp: >250 °C. ¹H NMR (500 MHz, CDCl₃) δ 7.73 (d, 2H, *J* = 8.5 Hz), 7.53 (dd, 2H, *J* = 8.5, 1.8 Hz), 7.44 (d, 1H, *J* = 7.5 Hz), 7.39–7.41 (m, 4H), 7.28–7.36 (m, 7H), 7.20 (td, 1H, *J* = 7.5, 1.0 Hz), 7.08 (td, 1H, *J* = 7.8, 1.2 Hz), 7.00 (td, 1H, *J* = 7.5, 1.0 Hz), 6.96 (td, 1H, *J* = 7.2, 0.8 Hz), 6.91 (d, 2H, *J* = 1.5 Hz), 6.69 (d, 1H, *J* = 7.0 Hz), 6.27 (d, 1H, *J* = 7.5 Hz). HRMS (APCI–TOF): Calcd for C₄₀H₂₄Br₂, 662.0245 (M⁺), found, 662.0246.

General procedure for bromination with CuBr₂/Al₂O₃. A solution of compounds **9–13** in carbon tetrachloride (50 mL per g) was added to CuBr₂/Al₂O₃ (3 equiv per reaction site). The reaction mixture was heated at reflux and monitored by TLC. After cooling to room temperature, the reaction mixture was filtered through a plug of silica gel. The solvents were removed under vacuum and the residual was subjected to column chromatography on silica gel eluted with hexane/DCM to afford compounds **14–18** as white solids.

Compound **14** was prepared following the reported procedure.¹⁵

Compound **15** (99%). Mp: >250 °C. ¹H NMR (500 MHz, CDCl₃) δ 7.55 (d, 1H, *J* = 1.5 Hz), 7.45 (d, 1H, *J* = 1.5 Hz), 7.40 (d, 4H, *J* = 9.0 Hz), 7.20–7.30 (m, 12H), 7.09 (d, 4H, *J* = 8.5 Hz), 7.03 (d, 1H, *J* = 8.0 Hz), 6.94 (d, 1H, *J* = 8.0 Hz). ¹³C NMR (125 MHz, CDCl₃) δ 159.2, 158.3, 155.4, 153.8, 141.5, 140.4, 137.0, 136.5, 132.1, 131.0, 130.7, 129.9, 128.9, 128.3, 127.7, 122.4, 121.9, 121.7, 120.8, 120.6, 63.5, 62.4. HRMS (APCI–TOF): Calcd for C₄₀H₂₄Br₄, 819.8612 (M⁺), found, 819.8599.

Compound **16** (96%). Mp: >250 °C. ¹H NMR (500 MHz, CDCl₃) δ 7.55 (d, 1H, *J* = 1.5 Hz), 7.46 (d, 1H, *J* = 1.5 Hz), 7.13–7.43 (m, 20H), 7.03 (d, 1H, *J* = 8.0 Hz), 6.96 (d, 1H, *J* = 8.5 Hz). ¹³C NMR (125 MHz, CDCl₃) δ 159.3, 157.8, 155.7, 153.6, 143.4, 141.4, 136.9, 136.4, 131.2, 131.0, 130.8, 130.5, 129.0, 128.9, 127.7, 126.9, 123.2, 122.4, 121.7, 120.8, 120.7, 63.5, 62.6. HRMS (APCI–TOF): Calcd for C₄₀H₂₄Br₄, 819.8612 (M⁺), found, 819.8608.

Compound **17** (95%). Mp: >250 °C. ¹H NMR (500 MHz, CDCl₃) δ 7.73 (d, 2H, *J* = 8.0 Hz), 7.54–7.56 (m, 3H), 7.31–7.38 (m, 11H), 7.12 (d, 1H, *J* = 8.0 Hz), 7.09 (dd, 1H, *J* = 8.0, 1.5 Hz), 6.89 (d, 2H, *J* = 1.5 Hz), 6.80 (d, 1H, *J* = 2.0 Hz), 6.11 (d, 1H, *J* = 8.0 Hz). ¹³C NMR (125 MHz, CDCl₃) δ 158.7, 153.7, 150.3, 146.0, 141.6, 140.0, 138.4, 135.7, 132.0, 131.4, 130.8, 129.0, 128.7, 128.2, 127.8, 127.1, 126.9, 122.3, 122.2, 122.0, 120.8, 120.6, 120.5, 64.2, 62.2. HRMS (APCI–TOF): Calcd for C₄₀H₂₂Br₄, 817.8455 (M⁺), found, 817.8438.

Compound **18** (92%). Mp: >250 °C. ¹H NMR (500 MHz, CDCl₃) δ 7.53 (d, 2H, *J* = 1.5 Hz), 7.23–7.28 (m, 22H), 7.01 (d, 2H, *J* = 8.0 Hz). ¹³C NMR (125 MHz, CDCl₃) δ 159.3, 154.9, 141.7, 137.2, 130.6, 128.8, 128.6, 128.4, 127.5, 122.1, 120.4, 63.4. HRMS (APCI–TOF): Calcd for C₄₀H₂₆Br₂, 664.0401 (M⁺), found, 664.0381.

Compound **19** was prepared from 2,7-dibromo-9-*H*-fluorene following the reported procedure.²⁰

General procedure for the Buchwald–Hartwig amination.

A Schlenk tube, charged with the corresponding substrate bromide (**14–19**), bis(4-methoxyphenyl)amine (1.5 equiv to C–Br bond), KO^t-Bu (1.2 equiv to amine), Pd(dba)₂ or Pd₂(dba)₃ (5% mol Pd per C–Br bond), and *t*-Bu₃P•HBF₄ (2 equiv to Pd), was evacuated and back-filled with nitrogen three times and dry toluene (25 mL per g substrate bromide). The reaction mixture was stirred at 40 °C for 30 min and then heated at reflux for 48 h before cooling to room temperature. After removal of solvent under vacuum, the residual was flowed through a short column of silica gel with hexane/DCM (plus 1% triethylamine). Preparative gel permeation chromatography (Tol, refraction index detector) gave the product.

Compound **1** (a yellow solid, 94%). Mp: 173–177 °C. ¹H NMR (500 MHz, C₆D₆) δ 7.68 (d, 1H, *J* = 2.0 Hz), 7.60 (d, 1H, *J* = 2.0 Hz), 7.48–7.50 (m, 4H), 7.44 (d, 4H, *J* = 9.0 Hz), 7.34 (d, 1H, *J* = 8.0 Hz), 7.19 (d, 1H, *J* = 8.5 Hz), 6.86–7.02 (m, 28H), 6.63–6.69 (m, 16H), 3.31 (s, 12H), 3.28 (s, 6H), 3.27 (s, 6H). ¹³C NMR (125 MHz, C₆D₆) δ 159.9, 159.0, 156.5, 156.2, 156.1, 154.6, 153.6, 148.0, 147.32, 147.25, 144.3, 141.8, 141.5, 135.6, 133.2, 132.7, 129.8, 129.1, 128.7, 127.3, 127.0, 126.6, 126.5, 121.4, 121.1, 120.8, 120.5, 120.3, 119.9, 119.8, 115.1, 115.0, 63.8, 62.5, 55.04, 55.00. HRMS (APCI–TOF): Calcd for C₉₆H₈₁N₄O₈, 1417.6054 (M + H⁺), found, 1417.6069.

Compound **2** (a yellow solid, 70%). Mp: 214–217 °C. ¹H NMR (500 MHz, C₆D₆) δ 7.60 (d, 1H, *J* = 2.5 Hz), 7.50 (d, 1H, *J* = 2.0 Hz), 7.42–7.43 (m, 2H), 7.34–7.36 (m, 4H), 7.13–7.17 (m, 2H), 7.06–7.08 (m, 4H), 6.86–7.01 (m, 25H), 6.76 (dd, 1H, *J* = 8.2, 2.2 Hz), 6.65–6.72 (m, 16H), 3.31 (s, 12H), 3.284 (s, 6H), 3.278 (s, 6H). ¹³C NMR (125 MHz, C₆D₆) δ 158.9, 158.5, 156.3, 156.2, 156.1, 154.0, 153.9, 149.1, 147.1, 144.8, 144.1, 141.9, 141.8, 141.4, 132.6, 132.4, 129.3, 129.0, 128.7, 126.9, 126.8, 126.4, 121.8, 121.5, 121.3, 121.0, 120.9, 120.1, 120.0, 119.5, 119.0, 115.0, 63.9, 63.6, 55.1, 55.0. HRMS (APCI–TOF): Calcd for C₉₆H₈₁N₄O₈, 1417.6054 (M + H⁺), found, 1417.6101.

Compound **3** (a yellow solid, 95%). Mp: 162–167 °C. ¹H NMR (500 MHz, C₆D₆) δ 7.54 (d, 1H, *J* = 2.0 Hz), 7.37–7.41 (m, 6H), 6.99–7.12 (m, 20H), 6.94 (d, 4H, *J* = 8.5 Hz), 6.83 (d, 4H, *J* = 9.0 Hz), 6.67–6.74 (m, 13H), 6.58–6.61 (m, 5H), 6.53 (d, 1H, *J* = 8.5 Hz). ¹³C NMR (125 MHz, C₆D₆) δ 159.3, 157.2, 156.2, 156.0, 155.9, 155.7, 151.4, 148.3, 147.4, 147.3, 143.9, 141.9, 141.7, 136.0, 134.2, 132.0, 128.8, 127.0, 126.4, 126.1, 122.2, 121.7, 121.0, 120.6, 120.5, 119.8, 119.6, 118.5, 117.7, 115.01, 114.97, 144.8, 64.1, 63.1, 55.1, 55.0, 54.9. HRMS (APCI–TOF): Calcd for C₉₆H₇₉N₄O₈, 1415.5898 (M + H⁺), found, 1415.5902.

Compound **4** (a yellow solid, 71%). Mp: 183–187 °C. ¹H NMR (500 MHz, C₆D₆) δ 7.65 (d, 1H, *J* = 2.0 Hz), 7.58 (d, 1H, *J* = 2.0 Hz), 7.50–7.54 (m, 8H), 7.30 (d, 1H, *J* = 8.5 Hz), 7.20 (d, 1H, *J* = 8.5 Hz), 6.64–7.06 (m, 20H), 6.61–6.65 (m, 8H), 3.28 (s, 6H), 3.26 (s, 6H), 2.44 (t, 4H, *J* = 7.8 Hz), 1.46–1.49 (m, 4H), 1.20–1.30 (m, 20H), 0.90 (t, 6H, *J* = 7.2 Hz). ¹³C NMR (125 MHz, C₆D₆) δ 159.4, 159.0, 156.2, 154.4, 153.7, 147.37, 147.33, 144.2, 141.80, 141.77, 141.55, 141.48, 132.9, 132.7, 129.14, 129.10, 128.8, 128.7, 127.0, 126.5, 121.3, 121.1, 120.7, 120.6, 119.8, 115.0, 63.8, 63.3, 55.0, 36.0, 32.3, 31.8, 29.91, 29.89, 29.7, 23.1, 14.4. HRMS (APCI–TOF): Calcd for C₈₄H₈₇N₂O₄, 1187.6666 (M + H⁺), found, 1187.6656.

Compound **5** (a yellow solid, 91%). Mp: 283–284 °C. ¹H NMR (500 MHz, C₆D₆): δ 7.62 (s, 2H), 7.48 (d, *J* = 7.0 Hz, 8H), 7.18 (d, *J* = 8.0 Hz, 2H), 7.02 (d, *J* = 7.0 Hz, 12H), 6.96 (d, *J* = 8.5 Hz, 8H), 6.87 (d, *J* = 8.0 Hz, 2H), 6.71 (d, *J* = 8.5 Hz, 8H), 3.58 (t, 7.5 Hz, 8H), 1.58 (quint, *J* = 7.5 Hz, 8H), 1.31 (quint, *J* = 7.5 Hz, 8H), 1.15–1.25 (m, 16H), 0.86 (t, *J* = 7.0 Hz, 12H). ¹³C NMR (125 MHz, C₆D₆): δ 158.9, 155.8, 153.7, 147.4, 144.0, 141.6, 132.5, 129.1, 128.7, 127.0, 126.5, 121.1, 120.5, 119.6, 115.5, 68.0, 63.7, 31.9, 29.6, 26.1, 23.0, 14.2. TOF MS (APCI⁺): 1243.7 [M]⁺; HRMS (APCI⁺) calcd for C₈₈H₉₄N₂O₄ (M): 1242.7208; found: 1242.7226.

Compound **6** (yellow solid). Mp: 163–164 °C. ¹H NMR (400 MHz, C₆D₆): δ 7.44 (s, 2H), 7.22 (d, *J* = 9.2 Hz, 8H), 7.15 (s, 4H), 6.83 (d, *J* = 9.2 Hz, 8H), 3.63 (t, *J* = 6.4 Hz, 8H), 1.41 (s, 12H), 1.60 (quint, *J* = 6.4 Hz, 8H), 1.34 (quint, *J* = 7.8 Hz, 8H), 1.15–1.29 (m, 16H), 0.86 (t, *J* = 6.9 Hz, 12H). ¹³C NMR (125 MHz, C₆D₆): δ 161.2, 156.2, 155.0, 147.4, 142.9, 133.1, 126.8, 122.1, 120.3, 118.2, 116.3, 68.7, 45.7, 32.5, 30.3, 26.7, 25.3, 23.6, 14.8. TOF MS (APCI⁺): 994.7 [M]⁺; HRMS (APCI⁺) calcd for C₆₈H₈₆N₂O₄ (M): 994.6582; found: 994.6578.

Compound **7** (a white solid, 57%). Mp: 91–93 °C. ¹H NMR (500 MHz, C₆D₆) δ 7.43 (d, 2H, *J* = 8.5 Hz), 7.32 (d, 2H, *J* = 2.0 Hz), 7.21 (d, 8H, *J* = 9.0 Hz), 7.14–7.16 (m, 2H), 6.79 (d, 8H, *J* = 9.0 Hz), 3.33 (s, 12H), 1.72–1.75 (m, 4H), 0.99–1.26 (m, 24H), 0.88 (t, 6H, *J* = 7.2 Hz). ¹³C NMR (125 MHz, C₆D₆) δ 156.2, 152.3, 148.0, 142.3, 135.5, 128.3, 126.4, 121.4, 120.0, 117.2, 115.1, 55.3, 55.0, 40.6, 32.3, 30.6, 29.85, 29.83, 24.6, 23.1, 14.4. HRMS (APCI–TOF): Calcd for C₅₇H₆₉N₂O₄, 845.5257 (M + H⁺), found, 845.5235.

UV–vis and PL spectra measurement. The UV–vis spectrum of the perovskite thin films on a PEDOT:PSS surface was recorded using a Jasco V-670 spectrophotometer. Photoluminescence of the PV film on glass was performed using a fluorescence spectrophotometer (HITACHI, F-4500).

Materials. Methylammonium iodide (MAI) was prepared following previous reports.¹¹ In a glove box (N₂ atmosphere), MAI, PbI₂ (TCI, 99.999%) and PbCl₂ (Aldrich, 99.999%) were dissolved in *N,N*-dimethylformamide (DMF, Tokyo Chemical Industry Co., 99.5%).

XRD diffraction measurements. The XRD experiment was performed on a Rigaku SmartLab X-ray diffractometer equipped with a scintillation counter. The measurement employed the Cu Kα line, focused radiation at 9 kW (45 kV, 200 mA) power using a 0.02° 2θ step scan from 3.0–35° with a scanning speed of 3° min⁻¹.

Evaluation of PV devices: Current–voltage sweeps were taken on a Keithley 2400 source measurement unit controlled by a computer. The light source used to determine the PCE was an AM 1.5G solar simulator system (Sumitomo Heavy Industries Advanced Machinery) with an intensity of 100 mW/cm². The SCs were masked with a metal aperture to define the active area of 4 mm².

Preparation of SCs. A fluorine-doped tin oxide (FTO) layer on a glass substrate was used for this study. Prior to the formation of the buffer layer, the patterned FTO glass was ultrasonically cleaned using a surfactant, rinsed with water and then finally given 3 min UV–ozone treatment. A 45-nm thick electron-transporting layer TiO_x was deposited by spin-coating (3000 rpm for 30 s) of the precursor solution (see materials section) and annealed at 500 °C for 30 min in air atmosphere.¹¹ To form the CH₃NH₃Pb_{1-x}Cl_x layer, a 40 wt %

precursor solution (4:1:1 mole ratio of CH₃NH₃I:PbI₂:PbCl₂) in DMF was spin-coated onto the TiO_x layer at 500 rpm for 3 s and 4000 rpm for 30 s. Further, it was annealed at 100 °C for 35 min in a nitrogen-filled glove box. The HTL (see materials section) 60 mg/mL in chlorobenzene with dopants (15 μL, 520 mg/mL Li-TFSI in CH₃CN and 22.5 μL TBP) was then deposited by spin coating (2200 rpm for 30 s). The top electrode (Au, 80 nm) was deposited through a metal shadow mask, which defined a 2 mm stripe pattern perpendicular to the ITO stripe.

ASSOCIATED CONTENT

Supporting Information. DFT calculations and UV–vis–NIR titration experiments, this material is available free of charge via the Internet at <http://pubs.acs.org>.

AUTHOR INFORMATION

Corresponding Author

*guoyunlong@chem.s.u-tokyo.ac.jp

*tsujiha@kanagawa-u.ac.jp

*nakamura@chem.s.u-tokyo.ac.jp

Present Addresses

†Prof. Hayato Tsuji, Faculty of Science, Kanagawa University, 2946 Tsuchiya, Hiratsuka, Kanagawa 259-1293, Japan.

†Dr. Qifan Yan, School of Chemistry and Molecular Engineering, East China University of Science and Technology, Meilong road 130, Shanghai 200237, China.

Notes

The authors declare no competing financial interests.

ACKNOWLEDGMENTS

We thank MEXT for financial support [KAKENHI 15H05754 to E.N., the Strategic Promotion of Innovative Research, JST to Y.G.; Q.Y. is grateful to the JSPS Postdoctoral Fellowship for Foreign Researchers (no. P13334)]. We thank Dr. Nai-Ti Lin for synthesis of compound 6.

REFERENCES

- (1) (a) Mayorga Burrezo, P.; Zhu, X.; Zhu, S.-F.; Yan, Q.; Lopez Navarrete, J. T.; Tsuji, H.; Nakamura, E.; Casado, J. *J. Am. Chem. Soc.* **2015**, *137*, 3834–3843. (b) Zhu, X.; Tsuji, H.; Lopez Navarrete, J. T.; Casado, J.; Nakamura, E. *J. Am. Chem. Soc.* **2012**, *134*, 19254.
- (2) (a) Roldán-Carmona, C.; Malinkiewicz, O.; Betancur, R.; Longo, G.; Mombblona, C.; Jaramillo, F.; Camacho, L.; Bolink, H. *J. Energy Environ. Sci.* **2014**, *7*, 2968. (b) Guo, Y.; Shoyama, K.; Sato, W.; Nakamura, E. *Adv. Energy Mater.* **2016**, *6*, 1502317.
- (3) (a) Kojima, A.; Teshima, K.; Shirai, Y.; Miyasaka, T. *J. Am. Chem. Soc.* **2009**, *131*, 6050. (b) Nishimura, H.; Ishida, N.; Shimazaki, A.; Wakamiya, A.; Saeki, A.; Scott, L. T.; Murata, Y. *J. Am. Chem. Soc.* **2015**, *137*, 15656–15659. (c) Grätzel, M. *Nat. Mater.* **2014**, *13*, 838. (d) Green, M. A.; Ho-Baillie, A.; Snaith, H. J. *Nat. Photon* **2014**, *8*, 506. (e) Yin, W.-J.; Yang, J.-H.; Kang, J.; Yan, Y.; Wei, S.-H. *J. Mater. Chem. A* **2015**, *3*, 8926.
- (4) (a) Matsuo, Y.; Sato, Y.; Niinomi, T.; Soga, I.; Tanaka, H.; Nakamura, E. *J. Am. Chem. Soc.*, **2009**, *131*, 16048–16050. (b) Cf. <http://www.japantimes.co.jp/news/2016/02/07/business/tech/technology-improves-future-organic-solar-cells-looks-bright/#.V5rudo787yc>

- (5) (a) Burschka, J.; Pellet, N.; Moon, S. J.; Baker, R. H.; Gao, P.; Nazeeruddin, M. K.; Grätzel, M. *Nature* **2013**, *499*, 316. (b) Liu, M.; Johnston, M. B.; Snaith, H. J. *Nature* **2013**, *501*, 395.
- (6) Zhu, X.; Tsuji, H.; Yella, A.; Chauvin, A.-S.; Grätzel, M.; Nakamura, E. *Chem. Commun.* **2013**, *49*, 582.
- (7) Morales-Vidal, M.; Boj, P. G.; Villalvilla, J. M.; Quintana, J. A.; Yan, Q.; Lin, N.-T.; Zhu, X.; Ruangsapichat, N.; Casado, J.; Tsuji, H.; Nakamura, E.; Diaz-Garcia, M. A. *Nat. Commun.* **2015**, *6*, 8458.
- (8) Sukegawa, J.; Schubert, C.; Zhu, X.; Tsuji, H.; Guldi, D. M.; Nakamura, E. *Nat. Chem.* **2014**, *6*, 899.
- (9) Sukegawa, J.; Tsuji, H.; Nakamura, E. *Chem. Lett.* **2014**, *43*, 699.
- (10) (a) Nelsen, S. F.; Ismagilov, R. F.; Powell, D. R. *J. Am. Chem. Soc.* **1996**, *118*, 6313. (b) We thank one of a reviewer for this interpretation of the ESR spectra.
- (11) (a) Guo, Y.; Liu, C.; Inoue, K.; Harano, H.; Tanaka, H.; Nakamura, E. *J. Mater. Chem. A* **2014**, *2*, 13827. (b) Guo, Y.; Liu, C.; Tanaka, H.; Nakamura, E. *J. Phys. Chem. Lett.* **2015**, *6*, 535. (c) Krishna, A.; Sabba, D.; Li, H.; Yin, J.; Boix, P. P.; Soci, C.; Mhaisalkar, S. G.; Grimsdale, A. C. *Chem. Sci.* **2014**, *5*, 2702. (d) Gratia, P.; Magomedov, A.; Malinauskas, T.; Daskeviciene, M.; Abate, A.; Ahmad, S.; Grätzel, M.; Getautis, V.; Nazeeruddin, M. K. *Angew. Chem. Int. Ed.* **2015**, *54*, 11409. (e) Li, M. H.; Hsu, C. W.; Shen, P. S.; Cheng, H. M.; Chi, Y.; Chen, P.; Guo, T. F. *Chem. Commun.* **2015**, *51*, 15518. (f) Park, S.; Heo, J. H.; Cheon, C. H.; Kim, H.; Im, S. H.; Son, H. J. *J. Mater. Chem. A* **2015**, *3*, 24215. (g) Liu, Y.; Hong, Z.; Chen, Q.; Chen, H.; Chang, W. H.; Yang, Y.; Song, T. B.; Yang, Y. *Adv. Mater.* **2016**, *28*, 440. (h) Rakstys, K. Saliba, M.; Gao, P.; Gratia, P.; Kamarauskas, E.; Paek, S.; Jankauskas, V.; Nazeeruddin, M. K. *Angew. Chem. Int. Ed.* **2016**, *55*, 7464.
- (12) Saragi, T. P. I.; Spehr, T.; Siebert, A.; Fuhrmann-Lieker, T.; Salbeck, J. *Chem. Rev.* **2007**, *107*, 1011.
- (13) Guo, Y.; Shoyama, K.; Sato, W.; Matsuo, Y.; Inoue, K.; Harano, K.; Liu, C.; Tanaka, H.; Nakamura, E. *J. Am. Chem. Soc.* **2015**, *137*, 15907–15914. Guo, Y.; Sato, W.; Shoyama, K.; Nakamura, E. *J. Am. Chem. Soc.*, **2016**, *138*, 5410–5416.
- (14) Still, W. C.; Kahn, M.; Mitra, A. *J. Org. Chem.* **1978**, *43*, 2923.
- (15) Zhu, X.; Tsuji, H.; Nakabayashi, K.; Ohkoshi, S.-i.; Nakamura, E. *J. Am. Chem. Soc.* **2011**, *133*, 16342.
- (16) Zhang, Y.; Lu, Z.; Desai, A.; Wulff, D. W. *Org. Lett.* **2008**, *10*, 5429.
- (17) Mills, N. S.; Tirla, C.; Benish, M. A.; Rakowitz, A. J.; Bebell, L. M.; Hurd, C. M. M.; Bria, A. L. M. *J. Org. Chem.* **2005**, *70*, 10709.
- (18) Fulmer, G. R.; Miller, A. J. M.; Sherden, N. H.; Gottlieb, H. E.; Nudelman, A.; Stoltz, B. M.; Bercaw, J. E.; Goldberg, K. I. *Organometallics* **2010**, *29*, 2176.
- (19) Kodomari, M.; Satoh, H.; Yoshitomi, S. *J. Org. Chem.* **1988**, *13*, 2093.
- (20) Hung, M.-C.; Liao, J.-L.; Chen, S.-A.; Chen, S.-H.; Su, A.-C. *J. Am. Chem. Soc.* **2005**, *127*, 14576.

